

Fast and Certified Bounding of Security-Constrained DCOPF via Interval Bound Propagation

Eren Tekeler, Samuel Chevalier
Electrical and Biomedical Engineering
University of Vermont
Burlington, VT, USA
{etekeler, schevali}@uvm.edu

Xiangru Zhong, Huan Zhang
Electrical and Computer Engineering
University of Illinois at Urbana-Champaign
Champaign and Urbana, IL, USA
{xiangru4, huanz}@illinois.edu

Abstract—Security-Constrained DC Optimal Power Flow (SC-DCOPF) is an important tool for transmission system operators, enabling economically efficient and physically secure dispatch decisions. Although CPU-based commercial solvers (e.g., Gurobi) can efficiently solve SC-DCOPF problems with a reasonable number of security constraints, their performance degrades rapidly as both system size and the number of contingencies grow into thousands, leading to a significant computational burden. This introduces a bottleneck for system operators who seek timely decision-making across a wide range of potential threats. In this paper, we design a computational graph representation of the SC-DCOPF-based market-clearing problem, inspired by the third ARPA-E Grid Optimization Competition (GO3). We are able to quickly bound the optimal solution of large-scale SC-DCOPF problems using a GPU-accelerated Neural Network verification tool called Interval Bound Propagation (IBP). Using IBP, we compute certified bounds with a maximum gap of 6.53% for instances up to 617 buses, while demonstrating scalability on challenging systems up to 8,316 buses with a runtime of approximately 0.07 seconds. These results demonstrate that IBP can provide high-quality solution bounds at very fast speeds, and it can help identify infeasibility drivers in challenging SC-DCOPF instances.

Index Terms—Security-constrained DCOPF, GPU-accelerated power systems optimization, Interval Bound Propagation, NN verification.

I. INTRODUCTION

The most recent Advanced Research Projects Agency-Energy (ARPA-E) Grid Optimization competition (GO3) focused on solving the multi-period Security Constrained Optimal Power Flow (SCOPF) problem [1]. The objective of this formulation was to maximize the market surplus while addressing various operational challenges. These challenges involved AC Optimal Power Flow (ACOPF) with soft constraints on nodal power imbalances and line flow violations, unit commitment, topology optimization, reserve constraints, generator start-up, and shut-down constraints. The multi-period aspect of the problem was explored across three different time horizons: real-time, day-ahead, and week-ahead. Furthermore, post-contingency line flows were evaluated using a linearized approximation of ACOPF, known as the DC Optimal Power Flow (DCOPF).

The GO3 test instances are designed with multiple dimensions of complexity, where problem size, number of contingencies, and time periods add further layers of difficulty, as

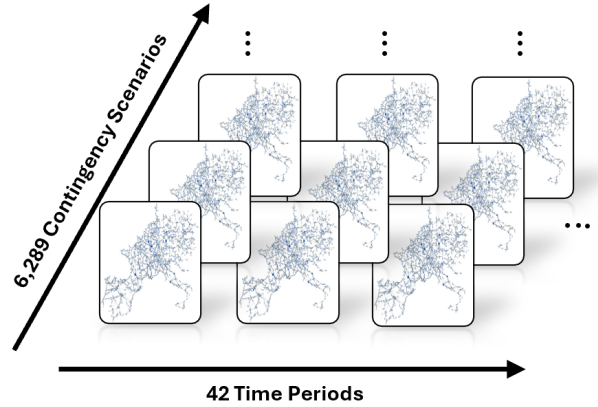


Fig. 1. Complexity dimensions of the largest GO3 test case (8,316-bus) solved in this paper.

illustrated in Fig. 1. Using traditional approaches, the problem requires solving large coupled systems of equations for each contingency scenario and time period, making them computationally challenging. In GO3, competitors predominantly employed decomposition and relaxation-based methods to solve the problems [1]. One competitor, quasigrad, employed a parallelized Adam-based approach on CPUs [2]; however, no team explored a GPU-based strategy that considered the full set of contingencies to address the problem. In this paper, we focus on posing and solving security-constrained DCOPF problems. Inspired by the GO3 formulation, we model the security constraints via DC power flow, while the base-case problem is modeled via soft constraints on nodal power imbalances and line flow violations; hard constraints are placed on the generation and demand limits. This formulation shares a structural similarity with the Neural Network (NN) verification problem, where the goal is to minimize or maximize NN outputs over a bounded input domain.

NN verification, which seeks to guarantee or deny the existence of adversarial inputs that violate some output metric, is a hard, nonconvex optimization problem. However, recent advances in GPU computing have enabled scalable and efficient verification techniques, which are broadly categorized as incomplete or complete. Incomplete methods, such as Interval Bound Propagation (IBP) [3], compute provable bounds on NN outputs over the entire input domain using

interval arithmetic, offering high speed and scalability at the cost of looser bounds. More advanced incomplete approaches, such as CROWN [4] and α -CROWN [5], construct convex relaxations to provide provable but not guaranteed global bounds, trading some speed for tighter guarantees. Complete verification methods, such as Branch and Bound [6], combine input domain partitioning with incomplete methods to compute provable global bounds given sufficient time.

In this paper, we use IBP to quickly compute relaxed bounds for hard power grid optimization problems. We refer to the resulting bounds as “certified” [7], in the sense that they are guaranteed convex relaxations of the true solution bounds. To compute these bounds, we cast the GO3-inspired SC-DCOPF as a computational graph, enabling our use of NN verification techniques and GPU acceleration. The key contributions are summarized as follows:

- 1) We translate the SC-DCOPF mathematical model into a computational graph in PyTorch, enabling GPU acceleration and compatibility with the NN verification framework α, β -CROWN.
- 2) Leveraging its scalability, computational speed, and tightness, we apply IBP to a range of GO3 test cases.
- 3) The certified bounds produced by IBP are used to infer the infeasibility of challenging SC-DCOPF instances.

In Sec. II, we walk through the formulation of the DCOPF, with a focus on the GO3-motivated SC-DCOPF model. Sec. III presents the NN Verification problem and introduces the SC-DCOPF computational graph design. We then discuss the results in Sec. IV and conclude with final remarks in Sec. V.

II. PROBLEM FORMULATION

In this section, we present the modified SC-DCOPF problem. We will use IBP to bound this model in later sections.

A. Market Clearing DCOPF

DCOPF is a linearized approximation of the ACOPF equations, used to solve for optimal generation dispatch in transmission systems. The approximation relies on the assumptions that the voltage angle difference between buses, $\theta_i - \theta_k$, is small (enabling trigonometric terms to be linearized using small-angle approximation), the resistive losses are negligible ($x \gg r$ in transmission lines), and that all bus voltage magnitudes satisfy $V_i \approx 1$. The DC power flow mappings are given by

$$\mathbf{p}_{\text{inj},r} = Y_{B,r} \boldsymbol{\theta}_r \quad (1a)$$

$$\mathbf{p}_f = Y_D E_r \boldsymbol{\theta}_r \quad (1b)$$

where the vector $\mathbf{p}_{\text{inj},r} \in \mathbb{R}^{n_b-1}$ represents the net nodal injections ($\mathbf{p}^g - \mathbf{p}^d$) with the row corresponding to the slack bus removed. The reduced nodal admittance matrix $Y_{B,r} \in \mathbb{R}^{(n_b-1) \times (n_b-1)}$ maps the reduced voltage angle vector $\boldsymbol{\theta}_r$ to the net injections. Moreover, the line flow vector, $\mathbf{p}_f \in \mathbb{R}^{n_l}$, is computed from the reduced voltage angle vector $\boldsymbol{\theta}_r$ through the diagonal line admittance matrix $Y_D \in \mathbb{R}^{n_l \times n_l}$ and the reduced incidence matrix $E_r \in \mathbb{R}^{n_l \times (n_b-1)}$. By left multiplying (1a)

with $Y_{B,r}^{-1}$, substituting the solution into (1b), and using the decomposition $Y_{B,r} = E_r^T Y_D E_r$, the reduced Power Transfer Distribution Factor (PTDF) matrix, Φ_r , is obtained as

$$\mathbf{p}_f = \underbrace{Y_D E_r (E_r^T Y_D E_r)^{-1}}_{\Phi_r} \mathbf{p}_{\text{inj},r}. \quad (2)$$

We note that the full PTDF matrix, $\Phi \in \mathbb{R}^{n_l \times n_b}$, provides a linear mapping from net nodal injections to the line flows. It is constructed by zero padding the *reduced* PTDF matrix Φ_r to account for the slack bus column: $\Phi = [0 \ \Phi_r]$.

Using this approximation, we formulate the following DCOPF problem, which maximizes social welfare by optimally dispatching generation and demand, while respecting power balance, line flow, generation, and demand constraints:

$$\max_{\mathbf{p}^g, \mathbf{p}^d} \sum_{j=1}^{n_d} \tau \mathbf{c}_j(\mathbf{p}_j^d) - \sum_{i=1}^{n_g} \tau \mathbf{g}_i(\mathbf{p}_i^g) \quad (3a)$$

$$\text{s.t. } \mathbf{1}^T \mathbf{p}^g - \mathbf{1}^T \mathbf{p}^d = \mathbf{0} \quad (3b)$$

$$\underline{\mathbf{p}}_f \leq \Phi(\mathbf{p}^g - \mathbf{p}^d) \leq \bar{\mathbf{p}}_f \quad (3c)$$

$$\underline{\mathbf{p}}_g \leq \mathbf{p}^g \leq \bar{\mathbf{p}}_g \quad (3d)$$

$$\underline{\mathbf{p}}_d \leq \mathbf{p}^d \leq \bar{\mathbf{p}}_d \quad (3e)$$

where $\mathbf{c} : \mathbb{R}^{n_d} \rightarrow \mathbb{R}^{n_d}$ and $\mathbf{g} : \mathbb{R}^{n_g} \rightarrow \mathbb{R}^{n_g}$ represent vectors of piece-wise linear cost functions, applied element-wise to demands and generations, $\mathbf{p}^d \in \mathbb{R}^{n_d}$ and $\mathbf{p}^g \in \mathbb{R}^{n_g}$, respectively. The scalar $\tau \in \mathbb{R}_{>0}$ denotes the duration of the dispatch interval (in h), which enables the objective value to be represented as total energy-based costs by scaling per-hour costs. For clarity, all upper and lower bounds on the constraints are specified element-wise, and the line flow bounds are symmetric, i.e., $\bar{\mathbf{p}}_f = -\underline{\mathbf{p}}_f$. We note that the load is generally flexible, so we refer to (3) as a market-clearing problem, consistent with the GO3 terminology.

B. Formulation of Soft-Constraints

In the GO3 formulation, rather than enforcing hard constraints on power balance and the line flows, as in (3), violations of constraints are captured using slack variables and penalized in the objective function using large violation cost coefficients (e.g., 10^6). This allows violations in the objective function to be expressed in monetary terms and combined with the market-based objective. The new power balance violation constraints are defined as

$$-\mathbf{s}_{\text{inj}} \leq (E^T \Phi - \mathbf{I})(\mathbf{p}^g - \mathbf{p}^d) \leq \mathbf{s}_{\text{inj}} \quad (4a)$$

$$\mathbf{s}_{\text{inj}} \geq \mathbf{0} \quad (4b)$$

where $\mathbf{s}_{\text{inj}} \in \mathbb{R}^{n_b}$ is the slack variable that captures the base case power balance violations through the nodal power injections, effectively being the soft-constrained representation of (3b). It sums incoming and outgoing flows via $E^T \Phi(\mathbf{p}^g - \mathbf{p}^d)$ to balance the net injections caused by generation and demand, based on Kirchhoff’s Current Law. Similarly, the line flow violation soft constraints are given by

$$\Phi(\mathbf{p}^g - \mathbf{p}^d) \leq \bar{\mathbf{p}}_{f,b} + \mathbf{s}_{f,b} \quad (5a)$$

$$-\Phi(\mathbf{p}^g - \mathbf{p}^d) \leq \bar{p}_{f,b} + s_{f,b} \quad (5b)$$

$$s_{f,b} \geq 0 \quad (5c)$$

in which $s_{f,b} \in \mathbb{R}^{n_l}$ is the slack variable that compensates for the base case line flow violations. Line flows, $\Phi(\mathbf{p}^g - \mathbf{p}^d)$, can take both positive and negative values depending on the flow direction. Thus, flow constraints are expressed symmetrically to account for both upper and lower bounds ($\underline{p}_{f,b} = -\bar{p}_{f,b}$), enabling $s_{f,b}$ to capture the magnitude of the violation.

C. Formulation of Security-Constraints

In addition to the soft-constrained nodal power injection and line flow violations, the GO3 formulation incorporates soft security constraints to ensure system operability under a set of N-1 contingencies by accounting for potential line flow violations in each contingency. However, incorporating all contingencies into the SC-DCOPF problem is computationally challenging, as each contingency requires inverting a new $Y_{B,r}$ matrix to obtain an updated contingency PTDF matrix which could map the net nodal injections to line flows. To overcome this, we model the admittance matrix associated with a given contingency as

$$Y_{B,r}^i = E_r^T Y_D E_r + e_i y_i e_i^T. \quad (6)$$

In (6), $Y_{B,r}^i$ represents a nodal admittance matrix with its i^{th} line removed. Via the Woodbury matrix identity [8], this matrix is computed using a rank-1 update applied to $Y_{B,r}$, where $e_i \in \mathbb{R}^{n_b-1}$ is the i^{th} row of E_r and scalar y_i is the negative of the i^{th} diagonal element of Y_D . The outer product $e_i y_i e_i^T$ forms a rank-1 matrix that effectively removes the line admittance of the i^{th} line from $Y_{B,r}$. By expanding (2) using the decomposition in (6) and introducing the matrix M_i to cancel the i^{th} diagonal element of Y_D , the contingency flows can be expressed as

$$\mathbf{p}_{f,c}^i = M_i Y_D E_r \underbrace{(E_r^T Y_D E_r + e_i y_i e_i^T)^{-1}}_{Y_{B,r}^i} \mathbf{p}_{\text{inj},r}, \quad (7)$$

where $\mathbf{p}_{f,c}^i$ denotes the contingency flow vector associated with an outage at the line i . The $M_i \in \mathbb{R}^{n_l \times n_l}$ is an identity matrix with its i^{th} diagonal element set to zero, effectively removing the corresponding line admittance from Y_D . However, computing (7) is expensive due to the need for inverse computation for each contingency. To accelerate contingency flow computations, the Sherman–Morrison theorem is applied, leveraging (6) to compute the inverse of the rank-1 updated matrix as

$$Y_{B,r}^{i-1} = Y_{B,r}^{-1} - \frac{Y_{B,r}^{-1} e_i y_i e_i^T Y_{B,r}^{-1}}{1 + e_i^T Y_{B,r}^{-1} e_i y_i} \quad (8)$$

such that the formulation enables efficient computation of the rank-1 updated matrix ($Y_{B,r}^i$) inverse using only the inverse of the base nodal admittance matrix $Y_{B,r}$, avoiding the need to recompute a full matrix inverse for each contingency scenario. Substituting this into (7) and simplifying, we get

$$\mathbf{p}_{f,c}^i = M_i \Phi_i \mathbf{p}_{\text{inj},r} - M_i Y_D E_r \mathbf{u}_i g_i (\mathbf{u}_i^T \mathbf{p}_{\text{inj},r}). \quad (9)$$

In (9), $\mathbf{u}_i \in \mathbb{R}^{n_b-1}$ is defined as $\mathbf{u}_i = Y_{B,r}^{-1} e_i$ and consequently, $\mathbf{u}_i^T = e_i^T Y_{B,r}^{-1}$ due to the square symmetric nature of the $Y_{B,r}^{-1}$ matrix. Additionally, the scalar term is simplified as $g_i = \frac{y_i}{1 + e_i^T \mathbf{u}_i y_i}$. To improve computational efficiency by avoiding forming the outer product $\mathbf{u}_i \mathbf{u}_i^T$, the second term is decomposed into $M_i Y_D E_r \mathbf{u}_i g_i$ and $(\mathbf{u}_i^T \mathbf{p}_{\text{inj},r})$, resulting in a vector-scalar product. The constants \mathbf{u}_i and g_i are precomputed once for each contingency and stored in memory.

Contingency line flow violations are evaluated in a similar manner to (5); however, the associated slack variable is denoted as $s_{f,c}^i \in \mathbb{R}^{n_l}$ for contingency at line i and the flow limits are enforced element-wise with $\bar{p}_{f,c}$. The total scalar contingency line flow violation is defined as

$$s_{f,c}^{\text{agg}} = \sum_{i=1}^{n_c} \mathbf{1}^T \mathbf{s}_{f,c}^i \quad (10)$$

where $s_{f,c}^{\text{agg}} \in \mathbb{R}$ represents the aggregated contingency line flow violations across all contingency scenarios, each computed efficiently with the rank-1 update formulation.

D. Objective Function Formulation

The GO3 formulation is a multi-period problem by its nature due to time-dependent reserve and generation constraints. In the scope of this paper, intertemporal constraints are neglected, and the problem is modeled as a sequence of independent single-period optimizations. We formulate the modified market-clearing SC-DCOPF problem as

$$\begin{aligned} \max_{\substack{\mathbf{p}_g \leq \mathbf{p}^g \leq \bar{\mathbf{p}}_g \\ \mathbf{p}_d \leq \mathbf{p}^d \leq \bar{\mathbf{p}}_d}} \quad & \sum_{j=1}^{n_d} \tau \mathbf{c}_j(\mathbf{p}_j^d) - \sum_{i=1}^{n_g} \tau \mathbf{g}_i(\mathbf{p}_i^g) - \tau e^{\text{inj}} \mathbf{1}^T \mathbf{s}^{\text{inj}} \\ & - \tau e^{\text{f}} \mathbf{1}^T \mathbf{s}_{f,b} - \tau e^{\text{f}} s_{f,c}^{\text{agg}}. \end{aligned} \quad (11)$$

This corresponds to the soft constrained representation of (3a). The penalty coefficients, $e^{\text{inj}}, e^{\text{f}} \in \mathbb{R}_{\gg 0}$ expressed in dollars per energy (\$/pu-h), serve to penalize the base-case nodal injection violations, base-case line flow violations, and contingency flow violations in the objective function. By incorporating the coefficients for violations, all terms are effectively represented in dollars (\$) in the objective function.

III. PROXY NN MODEL

We seek to efficiently bound the solution to (11). In this section, we do so by (i) converting (11) to a compute graph, and (ii) applying GPU-accelerated IPB. First, we briefly review the problem of NN verification and IPB.

A. Formal Verification of Neural Networks

In an L -Layer NN mapping $\text{NN}(\cdot) : \mathbb{R}^{n_1} \rightarrow \mathbb{R}^{n_L}$, let the input be $\mathbf{x} \in \mathbb{R}^{n_1}$. The pre-activation layer output of the i^{th} layer of $\text{NN}(\mathbf{x})$ is given by

$$\mathbf{x}^{(i)} = W^{(i-1)} \hat{\mathbf{x}}^{(i-1)} + \mathbf{b}^{(i-1)} \quad (12)$$

where $\hat{\mathbf{x}}^{(i)} = \sigma(\mathbf{x}^{(i)})$ represents the post-activation output and the input layer is $\mathbf{x} = \mathbf{x}^{(1)}$, and $i \in \{2, 3, 4, \dots, L\}$. The input is $\mathbf{x} \in C$, where set C defines a region bounded by a ℓ_p norm

ball constraint, $C = \{\mathbf{x} \mid \|\mathbf{x} - \mathbf{x}_0\|_p \leq \epsilon\}$, centered at \mathbf{x}_0 with the radius of ϵ . The function, $h(\cdot)$, that takes $\text{NN}(\mathbf{x})$ and collapses it into a scalar, $h(\cdot) : \mathbb{R}^{n_L} \rightarrow \mathbb{R}^1$, can be formally composed into $f(\mathbf{x}) \triangleq h(\text{NN}(\mathbf{x}))$. The objective function of the NN verification problem can be defined as

$$\min_{\mathbf{x} \in C} f(\mathbf{x}). \quad (13)$$

Robustness is certified if the global minimum value satisfies $f(\mathbf{x}) > \alpha$ for all $\mathbf{x} \in C$, where α is a given constant. The formulation in (11) shares the same structure as (13), with $f(\mathbf{x})$ representing the objective function and C denoting the feasible region defined by generation and demand constraints. More specifically, in NN verification, the objective function defines a mapping from inputs to outputs through successive layers, characterized by weights, biases, and activation function interactions. Likewise, in the SC-DCOPF problem, the market surplus objective is constructed through sequential operations, where linear mappings interact with nonlinear operators during cost and violation computations. This similarity allows the problem to be formulated analogously to a NN verification task, enabling the use of GPU-assisted NN Verification methods.

B. Interval Bound Propagation

IBP propagates element-wise bounded inputs through each NN layer, conservatively computing element-wise output bounds. Let the input $\mathbf{x} \in \mathbb{R}^n$ be bounded by the ℓ_∞ norm with a positive element-wise perturbation margin ϵ . The interval that \mathbf{x} lies between is defined as $\underline{\mathbf{x}} \leq \mathbf{x} \leq \bar{\mathbf{x}}$, where $\underline{\mathbf{x}} = \mathbf{x} - \epsilon$ and $\bar{\mathbf{x}} = \mathbf{x} + \epsilon$ are lower and upper bounds. Defining mean $\mathbf{x}_\mu = \frac{1}{2}(\bar{\mathbf{x}} + \underline{\mathbf{x}})$ and the deviation $\mathbf{x}_\sigma = \frac{1}{2}(\bar{\mathbf{x}} - \underline{\mathbf{x}})$, the bounds can be propagated through the NN layer $\mathbf{y} = \sigma(W\mathbf{x} + \mathbf{b})$ as

$$\bar{\mathbf{y}} = \sigma(|W|\mathbf{x}_\sigma + W\mathbf{x}_\mu + \mathbf{b}) \quad (14a)$$

$$\underline{\mathbf{y}} = \sigma(-|W|\mathbf{x}_\sigma + W\mathbf{x}_\mu + \mathbf{b}) \quad (14b)$$

where $\sigma(\cdot)$ is any element-wise monotonic activation function [3]. The bounds $\bar{\mathbf{y}}$ and $\underline{\mathbf{y}}$ are “certified”, meaning there exists no $\mathbf{x} \in [\underline{\mathbf{x}}, \bar{\mathbf{x}}]$ such that $\underline{\mathbf{y}} \notin [\underline{\mathbf{y}}, \bar{\mathbf{y}}]$. Generally, IBP will loosely bound the true reachable set.

C. Computational Graph Formulation

Computational graphs represent the flow of operations and dependencies in NNs, enabling a structured way to perform forward and backward passes and trackable gradient computations. To leverage the NN verifier α, β -CROWN, the SC-DCOPF model is represented as a computational graph, translating the nodal power imbalance constraints in (4) as

$$s_{\text{inj}} = |(E^T \Phi - \mathbf{I})(\mathbf{p}^g - \mathbf{p}^d)| \quad (15)$$

where the slack term s_{inj} captures the nodal power imbalance violations. Similarly, the base case line flow violations in (5) can be formulated as

$$s_{\text{f,b}} = \max(|\Phi(\mathbf{p}^g - \mathbf{p}^d)| - \bar{p}_{\text{f,b}}, 0) \quad (16)$$

in which $s_{\text{f,b}}$ quantifies any flow exceeding the limit $\bar{p}_{\text{f,b}}$. The same formulation applies to the contingency line flow slack

variable $s_{\text{f,c}}^i$, using the contingency flow upper bounds $\bar{p}_{\text{f,c}}$. Additionally, for the GO3 test instances with hundreds or thousands of contingencies, a loop-free model implementation is essential for traceability of the computational graph and faster computation time. With pre-processing, (9) is reformulated as

$$P_{\text{f,c}} = M \otimes (\mathbf{1}(\Phi \mathbf{p}_{\text{inj}})^T) - B \otimes ((U \mathbf{p}_{\text{inj}}) \mathbf{1}^T). \quad (17)$$

$M \in \mathbb{R}^{n_{\text{ctg}} \times n_l}$ is the preprocessed contingency matrix, with each row being all ones except for the contingency line entry, which is zero. The outer product $\mathbf{1}(\Phi \mathbf{p}_{\text{inj}})^T$ replicates the line flow vector, $\Phi \mathbf{p}_{\text{inj}}$, across rows to match the number of contingencies. The element-wise (Hadamard) product, denoted by \otimes , sets the line flow corresponding to the contingency to zero. With a slight simplification, $M_i Y_{\text{DE}} \mathbf{u}_i g_i$ vector can be denoted as \mathbf{b}_i and can be stacked as $B = [\mathbf{b}_1 \mathbf{b}_2 \mathbf{b}_3 \dots \mathbf{b}_{n_{\text{ctg}}}]^T$, where $B \in \mathbb{R}^{n_{\text{ctg}} \times n_l}$. Additionally, using the full \mathbf{p}_{inj} vector requires zero padding for \mathbf{u}_i when building the U matrix. The padded vector $\mathbf{u}'_i = [0 \mathbf{u}_i^T]^T$ forms the matrix $U = [\mathbf{u}'_1 \mathbf{u}'_2 \mathbf{u}'_3 \dots \mathbf{u}'_{n_{\text{ctg}}}]^T$, where $U \in \mathbb{R}^{n_{\text{ctg}} \times n_b}$. This avoids explicit looping over all contingencies and eliminates the need to store each M_i separately, resulting in significant computational efficiency.

D. Cost Function Implementation

In the GO3 formulation, the cost functions for generators and demands are modeled as convex and concave piece-wise linear functions, respectively. Given a piece-wise linear curve whose i^{th} segment has slope a_i and horizontal shift b_i , the curve can be represented using ReLU activations via (18b):

$$F_i(x) = a_i \text{ReLU}(x - b_i) \quad (18a)$$

$$F_i^*(x) = \min(F_{i-1}^*(x) + F_i(x), U_i) \quad (18b)$$

where U_i is the cumulative upper bound of segment $i \in \{1, 2, \dots, n_{\text{seg}}\}$, and $F_0^*(x) = 0$. Equation (18a) applies the slope scaling and horizontal shift for each segment, while in (18b), individual ReLUs are combined through addition and clipped to enforce the piecewise limits.

IV. RESULTS

In this section, we present simulated test results for the instances collected from various divisions and events of the GO3 competition. Specifically, we compare the bound provided by IBP with the optimal LP solution computed by Gurobi. We refer to the difference between these solutions as a “gap”:

$$\text{gap} \triangleq \frac{\text{IBP} - \text{Gurobi}}{\text{Gurobi}}. \quad (19)$$

All experiments were performed on the Vermont Advanced Computing Center (VACC) using AMD EPYC 7763 CPUs and NVIDIA H200 GPUs. The GO3-inspired SC-DCOPF model was solved using Gurobi in Julia, which served as a benchmark. Computational graphs were built in PyTorch, and IBP computations were performed using the α, β -CROWN.

Fig. 2 illustrates the optimality gap statistics across the benchmarked system sizes. For each system size, we solved multiple test instances using Gurobi and computed bounds

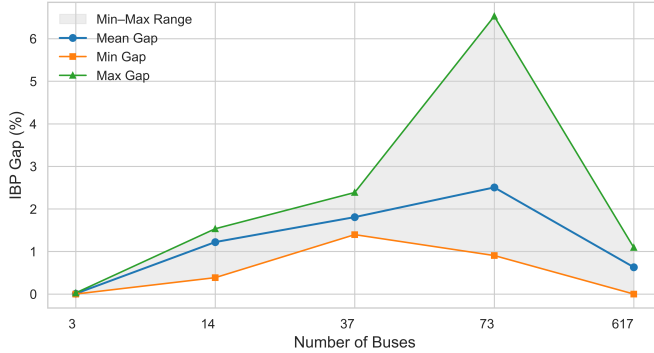


Fig. 2. IBP gap statistics across different benchmarked system sizes. Negative IBP upper bound scenarios are excluded.

using IBP. The mean gap remained below 3% for all systems, with the maximum gap occurring in a 73-bus instance at 6.53%. Additionally, in some test instances, the upper bounds computed by IBP are negative, meaning that no positive societal benefit can be obtained for the given input bounds. This can also be interpreted as a “guaranteed infeasibility¹”, arising either because generation costs exceed the value of the demands, or grid-physics are violated, or both. Identification of these instances eliminates the need to solve for the optimal dispatch, providing a substantial computational speed advantage.

TABLE I
IBP SPEEDUP SUMMARY FOR BENCHMARKED SYSTEM SIZES

| Number of Buses | Speedup (×) | | |
|-----------------|-------------|--------|--------|
| | Min | Mean | Max |
| 3 | 4.26 | 12.96 | 66.70 |
| 14 | 8.31 | 21.40 | 36.01 |
| 37 | 64.97 | 166.23 | 213.18 |
| 73 | 181.88 | 398.85 | 516.76 |
| 617 | 94.8k | 3.80M | 8.97M |

Table I presents statistics on the speedup achieved in bound computations and in identifying scenarios with negative net societal benefit. As the system size grows, IBP becomes increasingly advantageous, achieving speedups of up to 8.97 million times. Instances beyond 617 buses become challenging for Gurobi; in contrast, IBP scales efficiently, computing the bounds for systems up to 8,316 buses. All instances up to 6,717 buses were solved in batch for all time indices, while the 8,316-bus cases were solved serially for each time index due to memory limitations. Fig. 3 shows the distribution of runtimes to compute the bounds of a single time index across multiple test cases. Runtimes scale efficiently, from a 3-bus system with 2 contingencies to an 8,316-bus system with 6,289 contingencies, with mean runtimes reaching approximately 0.07 seconds.

¹No guaranteed infeasibility was observed for the 3, 14, 37, 73-bus systems with 0/25 each and 4,224-bus systems with 0/26. The 617 and 6,049-bus systems had 7/16 and 5/18 infeasible cases, respectively. The 1,576, 2,000, 6,717, and 8,316-bus systems exhibited 20/25, 25/25, 6/6, and 6/25 infeasible cases, respectively.

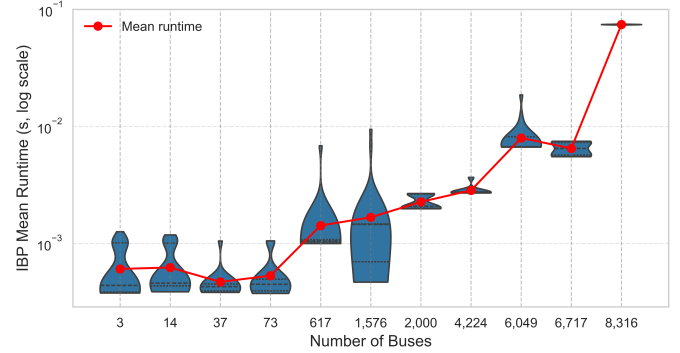


Fig. 3. Distribution of IBP mean runtimes in log scale across different system sizes.

V. CONCLUSION

In this paper, we formulated the GO3-inspired SC-DCOPF model as a computational graph to leverage GPU acceleration for bound computations via IBP. By employing α, β -CROWN, we evaluated IBP for its bound tightness, scalability, and ability to infer infeasibility. Our results demonstrate that it efficiently computes tight bounds and scales to one of the largest instances (8,316 buses with 6,289 contingencies) of the GO3 competition. Furthermore, we found that IBP bounds can identify infeasibility of test cases, significantly reducing computational overhead. Future work will investigate extending IBP within Branch and Bound frameworks to leverage its speed and scalability for computing global bounds on challenging power system problems.

REFERENCES

- [1] J. T. Holzer, S. Elbert, H. Mittelmann, R. O’Neill, and H. Oh, *Go competition challenge 3: Problem, solvers, and solution analysis*, 2024. arXiv: 2411.12033 [math.NA]. [Online]. Available: <https://arxiv.org/abs/2411.12033>
- [2] S. Chevalier, “A parallelized, adam-based solver for reserve and security constrained ac unit commitment,” *Electric Power Systems Research*, vol. 235, p. 110685, 2024, ISSN: 0378-7796. DOI: <https://doi.org/10.1016/j.epsr.2024.110685> [Online]. Available: <https://www.sciencedirect.com/science/article/pii/S0378779624005716>
- [3] S. Gowal et al., *On the effectiveness of interval bound propagation for training verifiably robust models*, 2019. arXiv: 1810.12715 [cs.LG]. [Online]. Available: <https://arxiv.org/abs/1810.12715>
- [4] H. Zhang, T.-W. Weng, P.-Y. Chen, C.-J. Hsieh, and L. Daniel, “Efficient neural network robustness certification with general activation functions,” *Advances in Neural Information Processing Systems*, vol. 31, pp. 4939–4948, 2018. [Online]. Available: <https://arxiv.org/pdf/1811.00866.pdf>
- [5] K. Xu et al., “Fast and Complete: Enabling complete neural network verification with rapid and massively parallel incomplete verifiers,” in *International Conference on Learning Representations*, 2021. [Online]. Available: <https://openreview.net/forum?id=nVZtXB16LN>
- [6] H. Zhang et al., “A branch and bound framework for stronger adversarial attacks of ReLU networks,” in *Proceedings of the 39th International Conference on Machine Learning*, vol. 162, 2022, pp. 26591–26604.
- [7] K. Xu et al., “Automatic perturbation analysis for scalable certified robustness and beyond,” *Advances in Neural Information Processing Systems*, vol. 33, 2020.
- [8] R. Horn and C. Johnson, *Matrix Analysis*. Cambridge University Press, 1990, ISBN: 9780521386326.